

SAMIC: Segment Anything with In-Context Spatial Prompt Engineering

Savinay Nagendra^{1,2} Kashif Rashid² Chaopeng Shen³ Daniel Kifer¹

¹Department of Computer Science and Engineering ³Department of Civil and Environmental Engineering

The Pennsylvania State University, University Park, Pennsylvania

²Schlumberger-Doll Research, Cambridge, Massachusetts

sxn265@psu.edu krashid@slb.com cshen@engr.psu.edu dkifer@cse.psu.edu

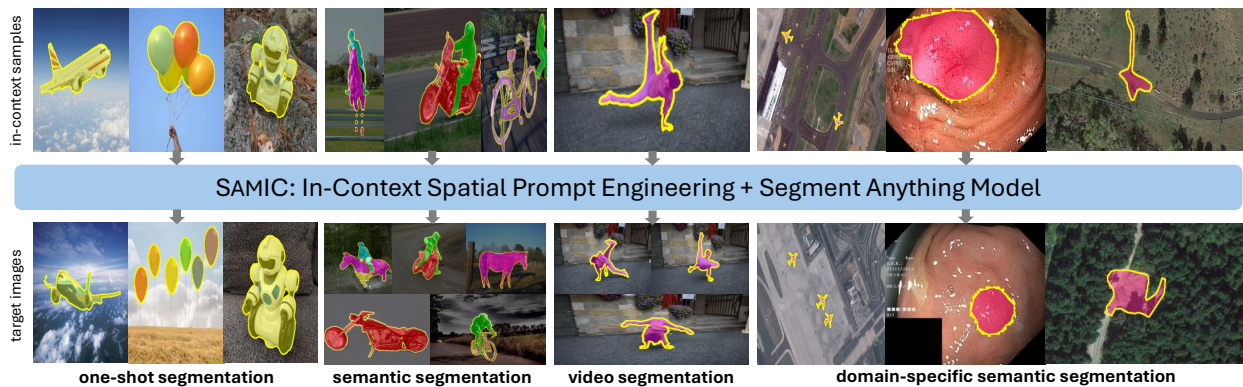


Figure 1. Qualitative results of SAMIC across diverse downstream segmentation tasks. SAMIC has two components, the in-context spatial prompt engineering module that predicts task-specific spatial prompts for target images (bottom row) by learning from a few in-context samples (top row), and the Segment Anything Model (SAM) that takes the spatial prompts as input to produce valid masks. SAMIC unifies a diverse set of downstream segmentation tasks including one-shot segmentation, semantic segmentation, video object segmentation and domain-specific semantic segmentation.

Abstract

Few-shot segmentation is the problem of learning to identify specific types of objects (e.g., airplanes) in images from a small set of labeled reference images. The current state of the art is driven by resource-intensive construction of models for every new domain-specific application. Such models must be trained on enormous labeled datasets of unrelated objects (e.g., cars, trains, animals) so that their “knowledge” can be transferred to new types of objects. In this paper, we show how to leverage existing vision foundation models (VFMs) to reduce the incremental cost of creating few-shot segmentation models for new domains. Specifically, we introduce SAMIC, a small network that learns how to prompt VFMs in order to segment new types of objects in domain-specific applications. SAMIC enables any task to be approached as a few-shot learning problem. At 2.6 million parameters, it is 94% smaller than the leading models (e.g., having ResNet 101 backbone with 45+ million parameters). Even using 1/5th of the training data provided

by one-shot benchmarks, SAMIC is competitive with, or sets the state of the art, on a variety of few-shot and semantic segmentation datasets including COCO-20ⁱ, Pascal-5ⁱ, PerSeg, FSS-1000, and NWPU VHR-10.

1. Introduction

Semantic segmentation is the task of identifying the pixels in images and videos belonging to specific objects (like polyps in medical datasets, airplanes in aerial images, etc.). It is not possible to create comprehensive training datasets, with pixel-level labeling, for all possible objects in existence. Hence, there is considerable interest in models that learn from small datasets, or even perform few-shot learning, where a model trained on one dataset is taught to recognize new types of objects from as few as 1-2 labeled reference images.

Many state-of-the-art few-shot benchmarks are dominated by relatively large models [12, 24, 85] (e.g., 45+

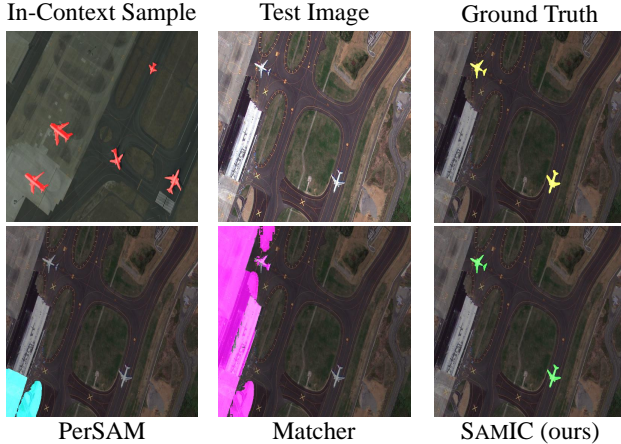


Figure 2. Comparison of top prompt engineering methods (PerSAM [86], Matcher [44]) for 1-shot airplane segmentation on a sample from NWPU VHR-10 [72]. The reference image contains masks of airplanes. The test image has similar airplanes, but the orientation and background differ.

million parameters) that are trained on massive datasets [37, 38, 70]. As a result, adding support for new domains is resource-intensive in terms of hardware and energy expenditures (e.g., one-shot segmentation models for animals need to be retrained to handle vehicles). On the other hand, the existence of Vision Foundation Models (VFMs) like the Segment Anything Model (SAM) [35] opens up the possibility that new domains can be supported by in-context learning (ICL) – specifically, prompt engineering. That is, much smaller models, trained on much smaller datasets, learn how to interact with a VFM to properly segment new classes of objects. In this spirit, we propose, a lightweight model named **SAMIC**¹ that is competitive with, and often outperforms, much larger models (and existing prompt engineering methods [44, 86]) on few-shot and small data benchmarks [29, 37, 55, 64, 70, 72].

VFMs [28, 35, 48, 59] now serve as backbones for multiple vision tasks, such as classification [80], object detection [48, 75, 89], and segmentation [14, 35, 59]. Given good *manual* prompts, they excel at many applications such as stable diffusion [66], visual query answering [2], and semantic/instance/panoptic segmentation [18, 20, 34]. In particular, SAM [35] is a VFM that can segment objects when manually provided with spatial prompts like pixel coordinates, bounding boxes, or raw masks.

Thus, instead of designing new custom models for computer vision tasks like semantic segmentation, one can turn it into a prompt engineering problem – training a model to give good prompts to SAM. Previous attempts at using ICL for segmentation [44, 74, 78, 79, 86] have had mixed suc-

cess. The most effective thus far are training-free spatial prompt engineering methods – PerSAM [86] and Matcher [44] that leverage frozen VFM encoders [35, 59] to extract embeddings. They create prompts in a new image by finding regions whose embeddings are similar to the labeled objects in the reference image. However, embeddings are complex and opaque objects that can capture information that may be irrelevant to a specific task. For these reasons, the training-free methods tend to be brittle – they can be distracted by changes in color, spatial orientation, and presence of other objects. An example is shown in Figure 2.

To get around this brittleness, methods need to be trained to understand what embeddings mean so that they can be used more effectively to learn about object boundaries, distinguishing instances, or grouping semantic regions. Thus SAMIC requires a small dataset of labeled objects to build “knowledge” it can transfer to new types of objects. Afterwards it can analyze one reference image containing new types of objects and design prompts for future images. Inspired by the success of the lightweight Hypercorrelation Squeeze Network (HSNet) [47] in few-shot learning, we adopt HSNet as the underlying architecture for SAMIC and we also created a custom annotation tool called **SAMBOX**.

SAMIC and SAMBOX operate as follows. To create an object mask for a reference image, a user would employ SAMBOX to add prompts to the reference image. SAMBOX displays the segmentation produced by SAM and allows the user to correct the prompts until the object is properly segmented. This is much faster than traditional annotation tools. SAMIC then places 2D Gaussians around these point prompts to create saliency-like heat maps [31] as a data pre-processing step. When new testing images start coming in, SAMIC takes that reference image, its heat map, and a new testing image, and then predicts the heat map for the testing image. Peaks in the predicted heatmaps are identified using a peak detection algorithm that we devised. These peaks become the prompts to the testing image, and are sent to SAM for segmentation.

Our main contributions are summarized as follows:

- We present SAMIC, a simple and highly efficient spatial prompt engineering framework that learns how to generate task-specific spatial point prompts for SAM. SAMIC uses a novel in-context saliency prediction architecture for predicting heat maps from which spatial point prompts are extracted using a peak detection algorithm.
- SAMIC is paired with a user-friendly annotation tool we call SAMBOX to facilitate the rapid collection of spatial point prompts for in-context learning. When we were preparing experiments for this paper, we found that using SAMBOX we could annotate images $6\times$ faster than with traditional tools like LabelMe [32].
- SAMIC uses an extremely small architecture (approximately $1/20^{\text{th}}$ the size of other state-of-the-art archi-

¹Source code will be released upon acceptance.

tures for 1-shot segmentation), making it very cost-efficient to train and deploy in new applications.

- SAMIC outperforms prior prompt-engineering methods and achieves state-of-the-art performance on a range of downstream tasks. To emphasize its data efficiency, SAMIC is only given 20% of the training data provided by the one-shot benchmarks, but is compared against methods that use all of the training data. For instance, SAMIC achieves state-of-the-art performance on ²Pascal-5ⁱ [70], and PerSeg [86] datasets with 1-shot mIoUs of 80.4%, and 97.5%, surpassing the previous state-of-the-art FP-Trans (ViT-B) [85] and Matcher [86] by +2.1% and +10.9% respectively. Additionally, SAMIC significantly surpasses Matcher [44], the previous state-of-the-art spatial prompt engineering method on domain-specific, real-world applications including gains of +35.3% on TSMU [55], +5.8% on Kvasir-SEG [29] and +18.5% on NWPU VHR-10 [72] datasets. On FSS-1000, SAMIC achieves 1-shot mIoU of 89%, while the state-of-the-art method VAT (ResNet-101) [85] with a much more complex model trained on 100% of the data achieves 90.3%.

2. Related Work

Vision Foundation Models (VFMs). In recent years, large-scale vision pre-training has driven significant advancements in VFMs, forming the basis for many state-of-the-art techniques [5, 10, 13, 19, 22, 23, 30, 35, 36, 54–57, 60, 65, 66, 82]. Vision-based models focus on tasks like distinguishing image or patch-level entities from different perspectives [10, 13, 22, 40, 49–53, 88] or reconstructing masked portions of images [5, 22]. For example, DINOv2 [59], a self-supervised VFM, surpasses OpenCLIP [28] in general-purpose feature extraction and exhibits strong visual feature matching. Of particular note, SAM [35] is a promptable VFM, pre-trained on the SA-1B dataset comprising 1B masks and 11M images, and uses precise spatial prompts to guide the model’s learning.

In-Context Segmentation. Recent research [4, 6, 44, 78, 79] has explored the use of in-context learning for segmentation tasks. Approaches like Painter [78] and SegGPT [79] implement in-context segmentation through image inpainting, building on the Masked Image Modeling (MIM) framework [23]. These models concatenate images and predictions into a 2×2 mosaic, predicting by reconstructing the masked regions. However, this process relies on a vision backbone that functions as both an image encoder and mask decoder, leading to high computational demands. Additionally, these methods face challenges in effectively utilizing pre-trained models due to input inconsistencies, resulting in slower convergence. PerSAM [86] and Matcher [44]

²Note that, for the Pascal=5ⁱ dataset, we do not consider SegGPT [79], because it trains on the testing data for Pascal-VOC dataset.

take a different approach by leveraging SAM [35] for in-context segmentation via prompting. They create one-shot, cross-image correspondences between examples and targets by computing cosine similarity matrices from generic VFM embeddings. However, these methods struggle to adapt to a wide range of downstream tasks due to the limitations of their prompt generation strategies. In contrast, SAMIC addresses these shortcomings by learning visual correspondences between in-context samples and target images, allowing for the prediction of task-specific spatial prompts.

3. Segmentation with SAMIC

The VFM SAM has a class-agnostic design [86] and therefore requires prompts in order to disambiguate what are the objects of interest and which image patches belong to the same (or different) objects. This presents an opportunity for models that learn *how* to prompt a VFM and is the motivation for SAMIC, a simple and efficient automated prompt engineering mechanism.

An RGB image or video frame with height H and width W can be represented as a tensor $\mathbf{I} \in \mathbb{R}^{3 \times H \times W}$. We let $\mathbf{I}(x, y)$ represent the RGB triple at location (x, y) in the image. The superscript t indicates that an image \mathbf{I}^t is a target/testing image. A spatial prompt \mathbf{P} is a set of points. An in-context sample is a set of K images and their associated spatial prompts: $\{(\mathbf{I}_1^c, \mathbf{P}_1), \dots, (\mathbf{I}_K^c, \mathbf{P}_K)\}$ where the spatial prompt $\mathbf{P}_i = \{(x_1, y_1), \dots, (x_{N_i}, y_{N_i})\}$ contains N_i points. For one-shot learning, $K = 1$. In a typical use-case, the in-context sample contains examples of a new type of object. The goal is to use these in-context samples to figure out how to automatically add spatial prompts to future images $\mathbf{I}_1^t, \mathbf{I}_2^t, \dots$ that contain such objects so that they can be segmented without any further human annotation.

3.1. Collecting unambiguous user prompts

To stream-line the annotation of in-context samples with good spatial prompts, we built an interactive annotation tool named SAMBOX (a snapshot of the tool is shown in Figure 3 with cyan colored point prompts). The purpose of SAMBOX is to guide the user into generating high quality, unambiguous prompts that will later provide a strong learning signal for SAMIC. SAMBOX interfaces with SAM and addresses some of its front-end limitations, especially with the segmentation of disjoint object instances in an image. For example, if one annotates two airplanes in an image using SAM’s front-end, SAM would return a segmentation that also includes the runway linking the airplanes together (SAMIC will also need to work around this limitation when predicting prompts). First, SAMBOX takes all of the images the user wants to annotate and runs them through SAM’s image encoder, saving the results to disk (this is a one-time pre-processing cost and takes ≈ 20 seconds per image on a Nvidia RTX 2080 Ti GPU). Then the user annotates each

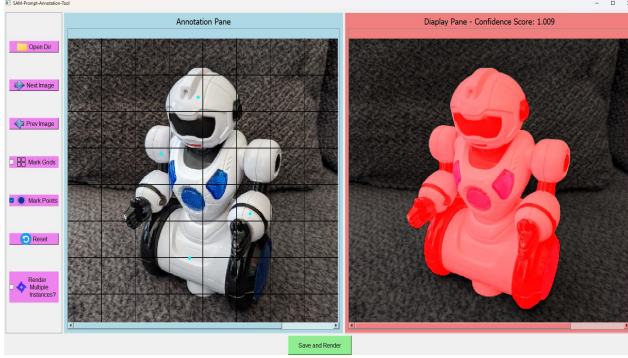


Figure 3. The SAMBOX annotation tool for rapid collection of unambiguous user prompts. With four user-provided spatial point prompts, SAMBOX outputs a mask with saturated confidence score of 1.009



Figure 4. Saliency-like 2D Gaussian heatmap generated from user-provided prompt with SAMBOX.

image sequentially via SAMBOX. If the user only wishes to annotate one object in an image, they would provide some point prompts or boxes and press “Save and Render”. SAMBOX sends these prompts to SAM, which responds with a mask and an ambiguity-aware confidence score.³ This information is presented to the user, who can then provide additional prompts, if necessary, to correct the segmentation.

The ambiguity score is critical to the success of SAMIC in one-shot segmentation. Even if SAM correctly segments an object, the user could keep adding point prompts until the confidence is nearly 1, as that represents a good, unambiguous prompt that SAMIC can learn from.

If the user wishes to segment multiple instances of an object in an image, SAMBOX would guide the user into providing prompts for each object. Prompts for each object are sent separately to SAM, to get multiple masks, which are then unioned by SAMBOX.

Collected point prompts are stored in a JSON file. Additionally, pixel-level masks are also stored, enabling the tool to function as a stand-alone rapid annotation platform for segmentation tasks. The tool supports instance and seman-

³For example, if the prompt is on a shirt, SAM does not know if the intention is to segment the shirt or the entire person wearing it, so the confidence score would be low.

tic segmentation tasks, making it highly scalable and adaptable for a wide range of applications. Using a standard RTX 2080 Ti GPU, a typical image can be annotated in less than 60 seconds, which, for us, was $\approx 5\times$ faster than manual pixel-wise annotation using a typical tool such as LabelMe [32]. For instance-segmentation or domain-specific tasks (where multiple objects have to be annotated), the tool accelerated our work by up to $\approx 15\times$.

3.2. Point Prompts to Saliency Heat Maps

Spatial point prompts are like indicators of the saliency of components of an object of interest. Thus, drawing inspiration from visual saliency prediction [31], we represent the spatial point prompts $\{(x_1, y_1), (x_2, y_2), \dots, (x_N, y_N)\}$ for an in-context image \mathbf{I}^c as a saliency-like heat map \mathbf{G} with the same height H and width W as \mathbf{I}^c . The heat map consists of Gaussians centered around each prompt. The intensity of the heatmap at point (x, y) is:

$$\mathbf{G}(x, y) = \sum_{k=1}^N \exp\left(-\frac{\left(\frac{x-x_k}{W}\right)^2 + \left(\frac{y-y_k}{H}\right)^2}{2\sigma^2}\right),$$

where σ controls the diffuseness of the Gaussians (we use $\sigma = 0.02$ throughout our experiments). The heatmap is then normalized (divided by the max value) to ensure every entry is $\in [0, 1]$. An example heatmap is shown in Figure 4.

3.3. SAMIC Architecture

The input to SAMIC is an in-context image with a heatmap along with a new testing image, and the output is a heatmap for the testing image. When there are $K > 1$ in-context images, they are fed to SAMIC one at a time with the testing image to get K heatmaps, which are then averaged. Then a peak-finding algorithm converts the heatmap into prompts (an overview of the process is shown in Figure 5). In principle, any architecture could be used with SAMIC, but we selected the Hypercorrelation Squeeze Network (HSNet) [47] (rather than, say, a transformer-based model [45]) because it is lightweight and has shown success in other few-shot learning applications [37]. For completeness, we briefly review the HSNet architecture.

Hypercorrelation Construction. Inspired by previous semantic matching approaches [43, 46], HSNet [47] leverages a comprehensive set of features from intermediate layers of a convolutional neural network to capture both semantic and geometric patterns of similarity between in-context and target images. In all experiments, ResNet-50 [21] is selected as the backbone network, which produces a sequence of L pairs of feature maps, denoted as F_l^c, F_l^t , for the reference and target images \mathbf{I}^c and \mathbf{I}^t , respectively. Here, F_l^c and F_l^t represent the feature maps obtained from the l^{th} layer of the network. To focus on relevant activations, each feature

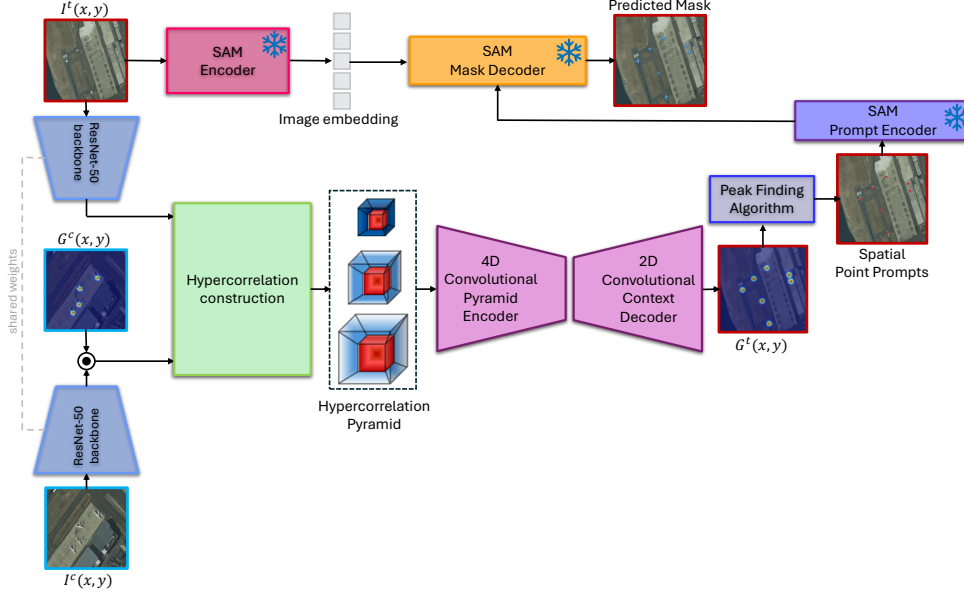


Figure 5. Overview of the SAMIC architecture. HSNet [47] is used as our in-context visual saliency prediction architecture to predict a saliency-like heat map with 2D Gaussians, representing location priors for task-specific spatial point prompts. A peak finding algorithm is used to extract a sequence of point prompts from the predicted heat map that are provided to SAM to generate segmentation masks.

map for the in-context image is masked with a saliency-like heatmap: $\hat{F}_l^c = F_l^c \odot \zeta(G^c)$, where \odot denotes the Hadamard product and $\zeta(\cdot)$ is a function that bilinearly interpolates the input tensor to match the spatial dimensions of the feature map. 4D correlation tensors between the two sets of feature maps are computed using cosine similarity:

$$\hat{C}_l(x^c, x^t) = \text{ReLU} \left(\frac{F_l^c(x^c) \cdot F_l^t(x^t)}{\|F_l^c(x^c)\| \|F_l^t(x^t)\|} \right),$$

where x^c and x^t represent the 2D spatial positions in F_l^c and F_l^t . These 4D correlation tensors are concatenated along the channel dimension to create a hypercorrelation tensor for each layer l , denoted as $C_l \in \mathbb{R}^{|L_l| \times H_l \times W_l \times H_l \times W_l}$. This process is repeated across different layers to obtain hypercorrelations at various spatial resolutions and depths, which are stacked together to form the hypercorrelation pyramid C .

4D-Convolutional Pyramid Encoder. The hypercorrelation pyramid C is compressed into a more compact feature map through the use of two types of building blocks: a squeezing block and a mixing block. Each block comprises three stages: multi-channel 4D convolution [16], group normalization [81], and ReLU [1] activation. In the squeezing block, large strides are applied to reduce the last two spatial dimensions of C while preserving the first two dimensions. The outputs from adjacent layers in the pyramid are combined using element-wise addition after upsampling the spatial dimensions of the upper layer. The mixing block then processes this combined output with 4D convolutions, facilitating the flow of relevant information from higher to

lower layers in a top-down manner. Lastly, average pooling is applied to produce the condensed representation Z of the hypercorrelation pyramid C .

2D-Convolutional Context Decoder The decoder network consists of a series of 2D convolutions, ReLU, and upsampling layers followed by softmax [8] function. The network takes the context representation Z and predicts $G^t \in [0, 1]^{1 \times H \times W}$, which is the predicted saliency-like heat map for the target image I^t .

3.4. Post-Processing: From Heatmaps to Prompts

We devise a peak detection algorithm to extract spatial point prompts P^t from a predicted saliency-like heatmap \hat{G}^t . This algorithm works as follows: First, \hat{G}^t is binarized with threshold $\tau = 0.5$ to get a binary map $B^t \in \{0, 1\}$. Second, contours are extracted from B^t using a contour detection algorithm [73] to identify connected components $R = \{R_1, R_2, \dots, R_N\}$ in B^t . For each connected component R_i , we calculate spatial moments [27] $M_{x,i}$, $M_{y,i}$, and the area A_i , where $M_{x,i} = \sum_{(x,y) \in R_i} x B_t(x,y)$, $M_{y,i} = \sum_{(x,y) \in R_i} y B_t(x,y)$ and $A_i = \sum_{(x,y) \in R_i} B_t(x,y)$. We then calculate the centroid (x_i, y_i) of each connected component R_i as $x_i = \frac{M_{x,i}}{A_i}$, $y_i = \frac{M_{y,i}}{A_i}$, which represents the peak of G_i . Finally, the extracted peaks $P^t = \{(x_1, y_1), (x_2, y_2), \dots, (x_N, y_N)\}$ become the spatial point prompts provided to SAM.

3.5. Loss Functions For Training

When training, let us denote the predicted and ground truth saliency-like heat maps as \hat{G} and G , respectively. Our loss function, adopted from standard visual saliency prediction methods [31, 45], has three components:

Kullback-Leibler Divergence (KLD) [9] measures the similarity between the two heat maps.

$$Loss_{KLD}(G, \hat{G}) = \sum_i G_i \log \left(\epsilon + \frac{G_i}{\hat{G}_i + \epsilon} \right), \quad (1)$$

where i denotes the location of pixels in the heat map, and $\epsilon = 1e^{-6}$ is a term that prevents division by 0.

One Minus Pearson’s Correlation Coefficient (CC) [17] is a statistical method that measures the linear correlation between two random variables.

$$Loss_{CC} = 1 - CC(\hat{G}, G) = 1 - \frac{\sigma(\hat{G}, G)}{\sigma(\hat{G}) \times \sigma(G)}, \quad (2)$$

where $\sigma(\hat{G}, G)$ denotes the covariance of \hat{G} and G while $\sigma(\hat{G})$ and $\sigma(G)$ are the standard deviations of \hat{G} and G , respectively. This loss function takes values in $[0, 2]$.

Normalized Scanpath Saliency (NSS) [62] is used to measure the average normalized saliency between two binary fixation maps, which are defined as follows. Let F denote the binarized version of the ground truth heat map G with threshold 0.5. That is, $F(x, y) = \mathbf{1}_{G(x,y) \geq 0.5}$. F is known as the fixation map.

$$Loss_{NSS}(\hat{G}, F) = \frac{1}{N} \sum_i (\bar{R}_i - \tilde{G}_i) \times F_i, \quad (3)$$

where $N = \sum_i F_i$ and $\tilde{G}_i = \frac{\hat{G}_i - \mu(\hat{G})}{\sigma(\hat{G})}$ and $\bar{R} = \frac{G - \mu(G)}{\sigma(G)}$.

The final loss function is a summation of all the components: $Loss = Loss_{KLD} + Loss_{CC} + Loss_{NSS}$.

4. Experiments

VFM and large-scale pre-trained models have created problems for the fair evaluation of computer vision algorithms on standard benchmarks, as these models are often trained on the entire benchmarks (including the testing sets). This can skew the results for methods built on top of them. This caveat is true for competing methods and also for SAMIC because it is not known exactly what the VFM SAM is trained on. However, based on dataset recency, we suspect that PerSeg [86] and TSMU [55] are least likely to have been used by SAM or large-scale pre-training models. In addition, NWPU VHR-10 [72] and Kvasir-SEG [29] are not cited by SAM [35] and so probably are not used by other pre-training models either. Thus, these 4 datasets may offer the fairest comparisons. We use a † to note when a model has a known potentially unfair advantage.

4.1. Datasets

Our experiments span nine benchmark ⁴datasets across four diverse tasks: few-shot segmentation, aerial segmentation, medical segmentation, and video object segmentation. Aerial and medical segmentation are classified as domain-specific segmentation tasks. For all datasets, SAMIC is only given 20% of the training data from each class.

Few-shot Segmentation is evaluated using the COCO-20ⁱ [58], Pascal-5ⁱ [70], FSS-1000 [37], and PerSeg [86] datasets. COCO-20ⁱ divides the 80 MSCOCO categories into four cross-validation folds, while Pascal-5ⁱ does the same for the 20 PASCAL VOC 2012 categories. FSS-1000 consists of 1,000 classes, each with 10 mask-annotated images. The dataset is split into 520 training classes, 240 for validation, and 240 for testing, supporting balanced and comprehensive evaluation across tasks. PerSeg is a personalized object detection dataset with 40 classes, which originates from Dreambooth [68] and is annotated by [86]. We follow the standard evaluation scheme in [47].

Video Object Segmentation (VOS) targets specific objects across video frames. We evaluate SAMIC on the test splits of DAVIS-16 [61] and DAVIS-17[64]. For training, we apply optical flow [26] to each video to extract the most dynamic frames, sampling 10 frames per video ($\approx 20\%$ of the training data). Frames are structured to maintain causality, with frame $t - 1$ used as reference for target frame t . Evaluation uses VOS metrics: J and F scores.

Domain-specific Segmentation. We evaluate SAMIC on domain-specific datasets that resemble real-world applications, rather than standard benchmarks or VFM pre-training datasets. We evaluate on two domain-specific tasks: (1) Aerial segmentation using the TSMU landslide [55], and NWPU VHR-10 [72] datasets, and (2) Medical segmentation using the Kvasir-SEG [29] dataset.

4.2. Implementation Details

We employ a ResNet-50 backbone [21] pre-trained on ImageNet [69]. Features are extracted at the end of each bottleneck before the ReLU [1] activation, yielding three pyramidal layers. The spatial size of reference and target images is set to 224×224 in our experiments, though it can be adjusted for custom datasets. The backbone network is frozen to prevent learning class-specific representations. SAMIC is trained with the Adam optimizer [33], using an initial learning rate of $1e-3$ and a batch size of 4. With only 2.6M learnable parameters, training on any custom dataset with a single class converges within 300 epochs (approx. 20 minutes on an NVIDIA 2080 Ti GPU), and early stopping is applied if training loss does not improve over 10 epochs.

⁴For additional details about the processing and construction of the datasets, please see supplementary material.

Methods	# learnable parameters	few-shot segmentation				aerial segmentation		medical segmentation	video object segmentation	
		COCO-20 ⁱ [58]	Pascal-5 ⁱ [70]	FSS-1000 [37]	PerSeg [68]	TSMU [55]	NWPU VHR-10 [72]	Kvasir-SEG [35]	DAVIS-16 [63]	DAVIS-17 [64]
		mIoU (1-shot)					<i>J & F</i> (1-shot)			
PerSAM (ViT-H) [86]	0	23.0	29.8	71.2	86.1	36.3	23.1	45.8	n/a	60.3
Matcher (ViT-G) [44]	0	52.7	76.9	87.0	86.6	52.9	51.6	63.5	86.1	79.5
SAMIC (ours)	2.6M	53.1	80.4	89.0	97.5	88.2	70.1	69.3	87.2	80.6

Table 1. Comparison of SAMIC with top spatial prompt engineering methods PerSAM [86] and Matcher [44] on 9 benchmark datasets spanning four diverse tasks of few-shot segmentation, aerial segmentation, medical segmentation and video object segmentation.

4.3. Quantitative Results

In our experiments, we evaluate methods from three categories: (i) *specialist segmentation models* that are fully supervised and trained to convergence on specific datasets, (ii) *in-context generalist segmentation models*, which are trained on major computer vision benchmarks and require in-context samples (reference image + reference mask) for segmentation, such as Painter [77] and SegGPT [79], and (iii) *in-context spatial prompt engineering models*, which generate spatial prompts and utilize SAM [35] as the segmenter. This third category includes (a) training-free methods such as PerSAM [86] and Matcher [44], and (b) SAMIC, which is trained on a small data subset for fast convergence and task-specific prompt generation. We report our results on the original test sets for all datasets.

Comparison of SAMIC with top SAM Prompting Methods. PerSAM [86] and Matcher [44] are the leading SAM-based spatial prompt engineering methods and are a natural comparison to SAMIC. Table 1 compares performance on nine benchmark datasets. On average, SAMIC outperforms Matcher by 1.5–2% on standard computer vision tasks like few-shot segmentation and VOS. The improvement is more substantial on domain-specific tasks, with gains of +35.3%, +18.5%, and +5.8% on TSMU, NWPU VHR-10 and Kvasir-SEG datasets. These results suggest that the prior methods can struggle in complex scenes with multiple objects, low saliency, varying scales, occlusions, and domain-specific textures.

Comparison of SAMIC with Specialist and In-Context Generalist Methods. We next compare against other generalist (prompt-based) and specialist models (traditional non-promptable models that predict segmentation masks). The results are shown in Table 2 and Table 3. On aerial segmentation (Table 2), SAMIC is the only generalist model that can outperform specialist models. It achieves state-of-the-art performance, getting gains of +19.1% and +10.8% on TSMU landslide [55] and NWPU VHR-10 [72] datasets. We observe from Table 3 that SAMIC significantly outperforms specialist models for few-shot segmentation on COCO-20ⁱ and Pascal-5ⁱ datasets with 53.1% and 80.4% mIoU. We include comparison with SegGPT but note that its training data includes the test sets of COCO and Pascal. On FSS-1000, SAMIC achieves comparable performance (89% mIoU) to the top specialist model VAT (90.3%),

Methods	# learnable parameters	TSMU [55]	NWPU VHR-10 [72]
		mIoU (1-shot)	
aerial segmentation specialist models			
U-Net [67]	30M	64.8	40.8
PSPNet [87]	47M	66.2	43.9
DeepLabV3+ [11]	43M	69.1	46.1
TSMU [55]	30M	68.3	n/a
WeSAM [84]	86M	n/a	35.5
PointSAM [41]	86M	n/a	59.3
in-context generalist segmentation models			
Painter (ViT-L) [78]	354M	32.8	20.8
SegGPT (ViT-L) [79]	354M	50.6	44.7
SAMIC (ours)	2.6M	88.2	70.1

Table 2. Comparison of SAMIC with current state-of-the-art specialist and in-context generalist segmentation models on TSMU Landslide [55] and NWPU VHR-10 [72] datasets from the task of aerial segmentation.

while have 1/20th as many parameters on 1/5 as much training data.

Limitations of SAMIC. It is also important to study limitations of a model and to understand when it might underperform. We have found that SAMIC underperforms in medical segmentation and VOS tasks, as shown in Table 4. In the case of Kvasir-SEG dataset, our examination of SAMIC’s prompts suggests that the prompts are good but that SAM struggles with typical characteristics of medical images, such as the low contrast of polyp images. Thus, improvements to SAM would lead to improvements to SAMIC. For VOS, SAMIC is not aware of temporal dependencies across video frames, which are crucial for high-accuracy visual object segmentation. With a one-shot setup, SAMIC falls short of matching the performance of specialized VOS models that are designed to take this information into account. These limitations highlight areas for further improvement in both SAMIC and SAM.

4.4. Ablation Study

We perform ablation experiments for establishing our design choice for SAMIC. We use a sub-sample of Pascal-5ⁱ as a validation set for ablation study.

Effect of depth in the Hypercorrelation Construction Block. As shown in Table 5, stacking 4D convolutional layers within the hypercorrelation construction block enhances performance up to a depth of three layers, after which per-

Methods	# learnable parameters	COCO-20 ⁱ [63]	Pascal-5 ⁱ [70]	FSS-1000 [37]
		mIoU (1-shot)		
few-shot segmentation specialist models				
HSNet (frozen ResNet-101) [47]	2.6M	41.2	68.7	86.5
VAT (ResNet-101) [25]	52M	41.3	72.4	90.3
FPTrans (ViT-B) [85]	101M	47.0	77.7	n/a
in-context generalist segmentation models				
Painter (ViT-L) [78]	354M	33.1	64.5	61.7
SegGPT (ViT-L) [79]	354M	56.1 [†]	83.2 [†]	85.6
SAMIC (ours)	2.6M	53.1	80.4	89.0

Table 3. Comparison of SAMIC with current state-of-the-art few-shot specialist and in-context generalist segmentation models on three benchmark few-shot datasets COCO-20ⁱ [58], Pascal-5ⁱ [70] and FSS-1000 [37]. [†]Note that SegGPT was trained on complete COCO and Pascal datasets, including the test sets.

Methods	# learnable parameters	medical segmentation	video object segmentation	
		Kvasir-SEG [29] mIoU (1-shot)	DAVIS-16 [63] <i>J & F</i> (1-shot)	DAVIS-17 [64] <i>J & F</i> (1-shot)
medical segmentation specialist models				
SS-Former-S [71]	30M	86.8	n/a	n/a
SS-Former-S + PRN [50]	32M	89.1	n/a	n/a
video segmentation specialist models				
SWEM (ResNet-50) [39]	58M	n/a	91.3	84.3
XMem (ResNet-50) [15]	62M	n/a	92.0	87.7
in-context generalist segmentation models				
Painter (ViT-L) [78]	354M	37.2	70.3	34.6
SegGPT (ViT-L) [79]	354M	43.7	83.7	75.6
SAMIC (ours)	2.6M	69.3	87.2	80.6

Table 4. Comparison of SAMIC with current state-of-the-art few-shot specialist and in-context generalist segmentation models on tasks of medical with Kvasir-SEG [29] dataset and video object segmentation with DAVIS-16 [63] and DAVIS-17 [64] datasets. This table highlights the limitations of using a prompt engineering method like SAMIC with a VFM like SAM, highlighting the need for specialist models for such hard domains.

#4D conv layers in Hypercorrelation Construction Block	pascal-5 ⁱ			
	mIoU (1-shot)	mIoU (5-shot)	# learnable parameters	inference time (ms)
1	62.1	67.6	0.2M	7
2	65.9	70.2	0.8M	16
3	66.1	70.4	2.6M	25
4	65.4	70.2	7.2M	72

Table 5. Effect of depth in the Hypercorrelation Construction Block.

formance gains plateau. Increasing depth also raises the number of learnable parameters and inference time. We select an optimal depth of three layers, achieving a model size of 2.6M parameters with a fast inference time of 25 ms, maximizing performance efficiently.

Effect of components of the loss function. The loss function of SAMIC comprises three components – KLD, CC, and NSS, as detailed in Section 3.5. KLD and CC help align the distributions, while NSS matches the intensity values between predicted and ground truth saliency maps. As shown in Table 6, using each component individually yields suboptimal performance. Combining KLD + NSS or CC + NSS improves results, but the highest performance is achieved when all three components are used together.

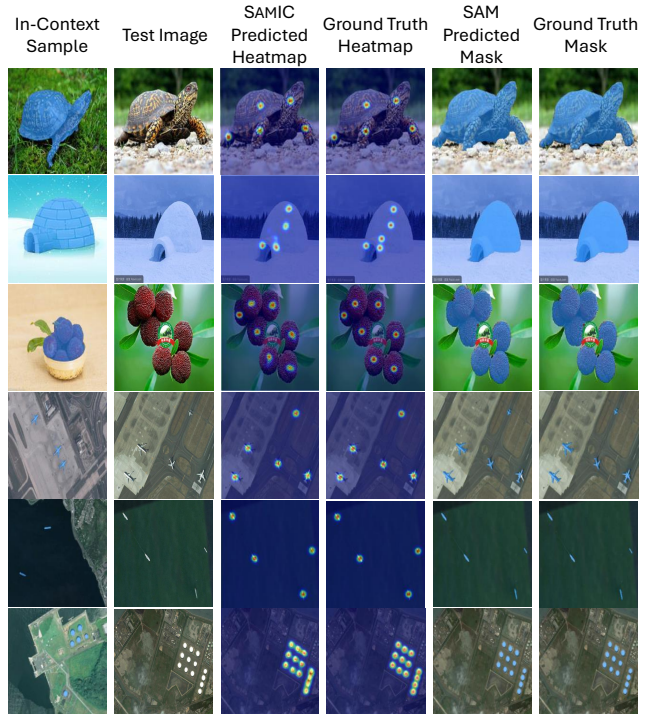


Figure 6. Qualitative results of SAMIC on FSS-1000 [37] and NWPU VHR-10 datasets [72], showing the predicted saliency heatmaps.

KLD	CCC	NSS	pascal-5 ⁱ	
			mIoU (1-shot)	mIoU (5-shot)
✓			58.6	61.2
	✓		52.8	53.3
		✓	42.7	43.9
✓		✓	64.9	68.1
	✓	✓	62.6	65.5
✓	✓	✓	66.1	70.4

Table 6. Effect of components of the loss function.

4.5. Qualitative Results

We demonstrate SAMIC’s effectiveness on diverse downstream tasks through qualitative results. In Figure 6, the few-shot learner (HSNet) within SAMIC effectively captures saliency heatmaps, generating high-quality spatial prompts for SAM. Figure 7 showcases SAMIC’s one-shot performance on the Pascal-5ⁱ, FSS-1000, and PerSeg datasets, clearly illustrating SAMIC’s ability to handle multiple objects (row 3), and perform part-object segmentation based on the given in-context sample (e.g., segmenting only the bike and not the person in row 2).

5. Conclusion

This paper introduces SAMIC, a compact 2.6M parameter network designed to prompt vision foundation models (VFMs) for efficient few-shot segmentation in new do-



Figure 7. Qualitative results of SAMIC for 1-shot segmentation on Pascal-5ⁱ [70], PerSeg [68], DAVIS-17 [64], TSMU [55] and Kvasir-SEG [29] datasets.

mains. Despite its small size, SAMIC achieves competitive or state-of-the-art performance across few-shot and semantic segmentation benchmarks using minimal training data. By leveraging VFMs, SAMIC enables any task to be approached as a few-shot learning problem and significantly reduces the cost of creating few-shot segmentation models for new domains. For additional details, please see supplementary material.

References

- [1] AF Agarap. Deep learning using rectified linear units (relu). *arXiv preprint arXiv:1803.08375*, 2018. 5, 6
- [2] Stanislaw Antol, Aishwarya Agrawal, Jiasen Lu, Margaret Mitchell, Dhruv Batra, C Lawrence Zitnick, and Devi Parikh. Vqa: Visual question answering. In *Proceedings of the IEEE international conference on computer vision*, pages 2425–2433, 2015. 2
- [3] David Arthur and Sergei Vassilvitskii. k-means++: The advantages of careful seeding. Technical report, Stanford, 2006. 14
- [4] Yutong Bai, Xinyang Geng, Kartikeya Mangalam, Amir Bar, Alan L Yuille, Trevor Darrell, Jitendra Malik, and Alexei A Efros. Sequential modeling enables scalable learning for large vision models. In *Proceedings of the IEEE/CVF Conference on Computer Vision and Pattern Recognition*, pages 22861–22872, 2024. 3
- [5] Hangbo Bao, Li Dong, Songhao Piao, and Furu Wei. Beit: Bert pre-training of image transformers. *arXiv preprint arXiv:2106.08254*, 2021. 3
- [6] Amir Bar, Yossi Gandelsman, Trevor Darrell, Amir Globerson, and Alexei Efros. Visual prompting via image inpainting. *Advances in Neural Information Processing Systems*, 35:25005–25017, 2022. 3
- [7] Malik Boudiaf, Hoel Kervadec, Ziko Imtiaz Masud, Pablo Piantanida, Ismail Ben Ayed, and Jose Dolz. Few-shot segmentation without meta-learning: A good transductive inference is all you need? In *Proceedings of the IEEE/CVF conference on computer vision and pattern recognition*, pages 13979–13988, 2021. 14
- [8] John Bridle. Training stochastic model recognition algorithms as networks can lead to maximum mutual information estimation of parameters. *Advances in neural information processing systems*, 2, 1989. 5
- [9] Zoya Bylinskii, Tilke Judd, Aude Oliva, Antonio Torralba, and Frédo Durand. What do different evaluation metrics tell us about saliency models? *IEEE transactions on pattern analysis and machine intelligence*, 41(3):740–757, 2018. 6
- [10] Mathilde Caron, Hugo Touvron, Ishan Misra, Hervé Jégou, Julien Mairal, Piotr Bojanowski, and Armand Joulin. Emerging properties in self-supervised vision transformers. In *Proceedings of the IEEE/CVF international conference on computer vision*, pages 9650–9660, 2021. 3
- [11] Liang-Chieh Chen. Rethinking atrous convolution for semantic image segmentation. *arXiv preprint arXiv:1706.05587*, 2017. 7
- [12] Shuai Chen, Fanman Meng, Runtong Zhang, Heqian Qiu, Hongliang Li, Qingbo Wu, and Linfeng Xu. Visual and textual prior guided mask assemble for few-shot segmentation and beyond. *IEEE Transactions on Multimedia*, 2024. 1
- [13] Ting Chen, Simon Kornblith, Mohammad Norouzi, and Geoffrey Hinton. A simple framework for contrastive learning of visual representations. In *International conference on machine learning*, pages 1597–1607. PMLR, 2020. 3
- [14] Bowen Cheng, Ishan Misra, Alexander G Schwing, Alexander Kirillov, and Rohit Girdhar. Masked-attention mask transformer for universal image segmentation. In *Proceedings of the IEEE/CVF conference on computer vision and pattern recognition*, pages 1290–1299, 2022. 2
- [15] Ho Kei Cheng and Alexander G Schwing. Xmem: Long-term video object segmentation with an atkinson-shiffrin memory model. In *European Conference on Computer Vision*, pages 640–658. Springer, 2022. 8
- [16] Christopher Choy, JunYoung Gwak, and Silvio Savarese. 4d spatio-temporal convnets: Minkowski convolutional neural

- networks. In *Proceedings of the IEEE/CVF conference on computer vision and pattern recognition*, pages 3075–3084, 2019. 5
- [17] Israel Cohen, Yiteng Huang, Jingdong Chen, Jacob Benesty, Jacob Benesty, Jingdong Chen, Yiteng Huang, and Israel Cohen. Pearson correlation coefficient. *Noise reduction in speech processing*, pages 1–4, 2009. 6
- [18] Gabriela Csurka, Riccardo Volpi, Boris Chidlovskii, et al. Semantic image segmentation: Two decades of research. *Foundations and Trends® in Computer Graphics and Vision*, 14(1-2):1–162, 2022. 2
- [19] Christopher Funk, Savinay Nagendra, Jesse Scott, Bharadwaj Ravichandran, John H Challis, Robert T Collins, and Yanxi Liu. Learning dynamics from kinematics: Estimating 2d foot pressure maps from video frames. *arXiv preprint arXiv:1811.12607*, 2018. 3
- [20] Abdul Mueed Hafiz and Ghulam Mohiuddin Bhat. A survey on instance segmentation: state of the art. *International journal of multimedia information retrieval*, 9(3):171–189, 2020. 2
- [21] Kaiming He, Xiangyu Zhang, Shaoqing Ren, and Jian Sun. Deep residual learning for image recognition. In *Proceedings of the IEEE conference on computer vision and pattern recognition*, pages 770–778, 2016. 4, 6
- [22] Kaiming He, Haoqi Fan, Yuxin Wu, Saining Xie, and Ross Girshick. Momentum contrast for unsupervised visual representation learning. In *Proceedings of the IEEE/CVF conference on computer vision and pattern recognition*, pages 9729–9738, 2020. 3
- [23] Kaiming He, Xinlei Chen, Saining Xie, Yanghao Li, Piotr Dollár, and Ross Girshick. Masked autoencoders are scalable vision learners. In *Proceedings of the IEEE/CVF conference on computer vision and pattern recognition*, pages 16000–16009, 2022. 3
- [24] Sunghwan Hong, Seokju Cho, Jisu Nam, and Seungryong Kim. Cost aggregation is all you need for few-shot segmentation. *arXiv preprint arXiv:2112.11685*, 2021. 1
- [25] Sunghwan Hong, Seokju Cho, Jisu Nam, Stephen Lin, and Seungryong Kim. Cost aggregation with 4d convolutional swin transformer for few-shot segmentation. In *European Conference on Computer Vision*, pages 108–126. Springer, 2022. 8
- [26] Berthold KP Horn and Brian G Schunck. Determining optical flow. *Artificial intelligence*, 17(1-3):185–203, 1981. 6
- [27] Ming-Kuei Hu. Visual pattern recognition by moment invariants. *IRE transactions on information theory*, 8(2):179–187, 1962. 5
- [28] Gabriel Ilharco, Mitchell Wortsman, Ross Wightman, Cade Gordon, Nicholas Carlini, Rohan Taori, Achal Dave, Vaishaal Shankar, Hongseok Namkoong, John Miller, et al. Openclip, 2021. 2, 3
- [29] Debesh Jha, Pia H Smedsrud, Michael A Riegler, Pål Halvorsen, Thomas de Lange, Dag Johansen, and Håvard D Johansen. Kvasir-seg: A segmented polyp dataset. In *International Conference on Multimedia Modeling*, pages 451–462. Springer, 2020. 2, 3, 6, 8, 9
- [30] Chao Jia, Yinfei Yang, Ye Xia, Yi-Ting Chen, Zarana Parekh, Hieu Pham, Quoc Le, Yun-Hsuan Sung, Zhen Li, and Tom Duerig. Scaling up visual and vision-language representation learning with noisy text supervision. In *International conference on machine learning*, pages 4904–4916. PMLR, 2021. 3
- [31] Sen Jia and Neil DB Bruce. Eml-net: An expandable multi-layer network for saliency prediction. *Image and vision computing*, 95:103887, 2020. 2, 4, 6
- [32] w kentaro. Labelme: Image polygonal annotation with python, 2021. 2, 4
- [33] Diederik P Kingma. Adam: A method for stochastic optimization. *arXiv preprint arXiv:1412.6980*, 2014. 6
- [34] Alexander Kirillov, Kaiming He, Ross Girshick, Carsten Rother, and Piotr Dollár. Panoptic segmentation. In *Proceedings of the IEEE/CVF conference on computer vision and pattern recognition*, pages 9404–9413, 2019. 2
- [35] Alexander Kirillov, Eric Mintun, Nikhila Ravi, Hanzi Mao, Chloe Rolland, Laura Gustafson, Tete Xiao, Spencer Whitehead, Alexander C Berg, Wan-Yen Lo, et al. Segment anything. In *Proceedings of the IEEE/CVF International Conference on Computer Vision*, pages 4015–4026, 2023. 2, 3, 6, 7, 13
- [36] Junnan Li, Ramprasaath Selvaraju, Akhilesh Gotmare, Shafiq Joty, Caiming Xiong, and Steven Chu Hong Hoi. Align before fuse: Vision and language representation learning with momentum distillation. *Advances in neural information processing systems*, 34:9694–9705, 2021. 3
- [37] Xiang Li, Tianhan Wei, Yau Pun Chen, Yu-Wing Tai, and Chi-Keung Tang. Fss-1000: A 1000-class dataset for few-shot segmentation. In *Proceedings of the IEEE/CVF conference on computer vision and pattern recognition*, pages 2869–2878, 2020. 2, 4, 6, 7, 8
- [38] Tsung-Yi Lin, Michael Maire, Serge Belongie, James Hays, Pietro Perona, Deva Ramanan, Piotr Dollár, and C Lawrence Zitnick. Microsoft coco: Common objects in context. In *Computer Vision—ECCV 2014: 13th European Conference, Zurich, Switzerland, September 6–12, 2014, Proceedings, Part V 13*, pages 740–755. Springer, 2014. 2
- [39] Zhihui Lin, Tianyu Yang, Maomao Li, Ziyu Wang, Chun Yuan, Wenhao Jiang, and Wei Liu. Swen: Towards real-time video object segmentation with sequential weighted expectation-maximization. In *Proceedings of the IEEE/CVF Conference on Computer Vision and Pattern Recognition*, pages 1362–1372, 2022. 8
- [40] Jiangtao Liu, Chaopeng Shen, Te Pei, Kathryn Lawson, Daniel Kifer, Savinay Nagendra, and Srikanth Bangere Manjunatha. A new rainfall-induced deep learning strategy for landslide susceptibility prediction. In *AGU Fall Meeting Abstracts*, pages NH35E–0504, 2021. 3
- [41] Nanqing Liu, Xun Xu, Yongyi Su, Haojie Zhang, and Heng-Chao Li. Pointsam: Pointly-supervised segment anything model for remote sensing images. *arXiv preprint arXiv:2409.13401*, 2024. 7
- [42] Yongfei Liu, Xiangyi Zhang, Songyang Zhang, and Xuming He. Part-aware prototype network for few-shot semantic segmentation. In *Computer Vision—ECCV 2020: 16th European Conference, Glasgow, UK, August 23–28, 2020, Proceedings, Part IX 16*, pages 142–158. Springer, 2020. 14

- [43] Yanbin Liu, Linchao Zhu, Makoto Yamada, and Yi Yang. Semantic correspondence as an optimal transport problem. In *Proceedings of the IEEE/CVF Conference on Computer Vision and Pattern Recognition*, pages 4463–4472, 2020. 4
- [44] Yang Liu, Muzhi Zhu, Hengtao Li, Hao Chen, Xinlong Wang, and Chunhua Shen. Matcher: Segment anything with one shot using all-purpose feature matching. *arXiv preprint arXiv:2305.13310*, 2023. 2, 3, 7, 15
- [45] Jianxun Lou, Hanhe Lin, David Marshall, Dietmar Saupe, and Hantao Liu. Transalnet: Towards perceptually relevant visual saliency prediction. *Neurocomputing*, 494:455–467, 2022. 4, 6
- [46] Juhong Min, Jongmin Lee, Jean Ponce, and Minsu Cho. Hyperpixel flow: Semantic correspondence with multi-layer neural features. In *Proceedings of the IEEE/CVF International Conference on Computer Vision*, pages 3395–3404, 2019. 4
- [47] Juhong Min, Dahyun Kang, and Minsu Cho. Hypercorrelation squeeze for few-shot segmentation. In *Proceedings of the IEEE/CVF international conference on computer vision*, pages 6941–6952, 2021. 2, 4, 5, 6, 8, 14
- [48] M Minderer, A Gritsenko, A Stone, M Neumann, D Weisenborn, A Dosovitskiy, A Mahendran, A Arnab, M Dehghani, Z Shen, et al. Simple open-vocabulary object detection with vision transformers. arxiv 2022. *arXiv preprint arXiv:2205.06230*, 2, 2022. 2
- [49] Savinay Nagendra. Thermal analysis for nvidia gtx480 fermi gpu architecture. *arXiv preprint arXiv:2403.16239*, 2024. 3
- [50] Savinay Nagendra and Daniel Kifer. Patchrefinenet: Improving binary segmentation by incorporating signals from optimal patch-wise binarization. In *Proceedings of the IEEE/CVF Winter Conference on Applications of Computer Vision*, pages 1361–1372, 2024. 8
- [51] Savinay Nagendra and Prapti Panigrahi. Emotion recognition from the perspective of activity recognition. *arXiv preprint arXiv:2403.16263*, 2024.
- [52] Savinay Nagendra, Nikhil Podila, Rashmi Ugarakhod, and Koshy George. Comparison of reinforcement learning algorithms applied to the cart-pole problem. In *2017 international conference on advances in computing, communications and informatics (ICACCI)*, pages 26–32. IEEE, 2017.
- [53] Savinay Nagendra, S Banagere Manjunatha, Chaopeng Shen, Daniel Kifer, and Te Pei. An efficient deep learning mechanism for cross-region generalization of landslide events. In *AGU Fall Meeting Abstracts*, pages NH030–0010, 2020. 3
- [54] S Nagendra, T Pei, S Banagere Manjunatha, G He, T Qiu, D Kifer, and C Shen. Cloud-based interactive database management suite integrated with deep learning-based annotation tool for landslide mapping. In *AGU Fall Meeting Abstracts*, pages NH030–0011, 2020. 3
- [55] Savinay Nagendra, Daniel Kifer, Benjamin Mirus, Te Pei, Kathryn Lawson, Srikanth Banagere Manjunatha, Weixin Li, Hien Nguyen, Tong Qiu, Sarah Tran, et al. Constructing a large-scale landslide database across heterogeneous environments using task-specific model updates. *IEEE Journal of Selected Topics in Applied Earth Observations and Remote Sensing*, 15:4349–4370, 2022. 2, 3, 6, 7, 9
- [56] Savinay Nagendra, Chaopeng Shen, and Daniel Kifer. Threshnet: Segmentation refinement inspired by region-specific thresholding. *arXiv preprint arXiv:2211.06560*, 2: 1, 2022.
- [57] Savinay Nagendra, Chaopeng Shen, and Daniel Kifer. Estimating uncertainty in landslide segmentation models. *arXiv preprint arXiv:2311.11138*, 2023. 3
- [58] Khoi Nguyen and Sinisa Todorovic. Feature weighting and boosting for few-shot segmentation. In *Proceedings of the IEEE/CVF International Conference on Computer Vision*, pages 622–631, 2019. 6, 7, 8
- [59] Maxime Oquab, Timothée Darcet, Théo Moutakanni, Huy Vo, Marc Szafraniec, Vasil Khalidov, Pierre Fernandez, Daniel Haziza, Francisco Massa, Alaaeldin El-Nouby, et al. Dinov2: Learning robust visual features without supervision. *arXiv preprint arXiv:2304.07193*, 2023. 2, 3
- [60] Te Pei, Savinay Nagendra, Srikanth Banagere Manjunatha, Guanlin He, Daniel Kifer, Tong Qiu, and Chaopeng Shen. Utilizing an interactive ai-empowered web portal for landslide labeling for establishing a landslide database in washington state, usa. In *EGU General Assembly Conference Abstracts*, pages EGU21–13974, 2021. 3
- [61] Federico Perazzi, Jordi Pont-Tuset, Brian McWilliams, Luc Van Gool, Markus Gross, and Alexander Sorkine-Hornung. A benchmark dataset and evaluation methodology for video object segmentation. In *Proceedings of the IEEE conference on computer vision and pattern recognition*, pages 724–732, 2016. 6
- [62] Robert J Peters, Asha Iyer, Laurent Itti, and Christof Koch. Components of bottom-up gaze allocation in natural images. *Vision research*, 45(18):2397–2416, 2005. 6
- [63] Felipe Pezoa, Juan L Reutter, Fernando Suarez, Martín Ugarte, and Domagoj Vrgoč. Foundations of json schema. In *Proceedings of the 25th international conference on World Wide Web*, pages 263–273, 2016. 7, 8
- [64] Jordi Pont-Tuset, Federico Perazzi, Sergi Caelles, Pablo Arbeláez, Alex Sorkine-Hornung, and Luc Van Gool. The 2017 davis challenge on video object segmentation. *arXiv preprint arXiv:1704.00675*, 2017. 2, 6, 7, 8, 9
- [65] Alec Radford, Jong Wook Kim, Chris Hallacy, Aditya Ramesh, Gabriel Goh, Sandhini Agarwal, Girish Sastry, Amanda Askell, Pamela Mishkin, Jack Clark, et al. Learning transferable visual models from natural language supervision. In *International conference on machine learning*, pages 8748–8763. PMLR, 2021. 3
- [66] Robin Rombach, Andreas Blattmann, Dominik Lorenz, Patrick Esser, and Björn Ommer. High-resolution image synthesis with latent diffusion models. In *Proceedings of the IEEE/CVF conference on computer vision and pattern recognition*, pages 10684–10695, 2022. 2, 3
- [67] Olaf Ronneberger, Philipp Fischer, and Thomas Brox. U-net: Convolutional networks for biomedical image segmentation, 2015. 7
- [68] Nataniel Ruiz, Yuanzhen Li, Varun Jampani, Yael Pritch, Michael Rubinstein, and Kfir Aberman. Dreambooth: Fine tuning text-to-image diffusion models for subject-driven generation. In *Proceedings of the IEEE/CVF conference*

- on computer vision and pattern recognition, pages 22500–22510, 2023. 6, 7, 9, 15
- [69] Olga Russakovsky, Jia Deng, Hao Su, Jonathan Krause, Sanjeev Satheesh, Sean Ma, Zhiheng Huang, Andrej Karpathy, Aditya Khosla, Michael Bernstein, et al. Imagenet large scale visual recognition challenge. *International journal of computer vision*, 115:211–252, 2015. 6
- [70] Amirreza Shaban, Shray Bansal, Zhen Liu, Irfan Essa, and Byron Boots. One-shot learning for semantic segmentation. *arXiv preprint arXiv:1709.03410*, 2017. 2, 3, 6, 7, 8, 9
- [71] Wentao Shi, Jing Xu, and Pan Gao. Ssformer: A lightweight transformer for semantic segmentation. In *2022 IEEE 24th International Workshop on Multimedia Signal Processing (MMSP)*, pages 1–5. IEEE, 2022. 8
- [72] Hao Su, Shunjun Wei, Min Yan, Chen Wang, Jun Shi, and Xiaoling Zhang. Object detection and instance segmentation in remote sensing imagery based on precise mask r-cnn. In *IGARSS 2019-2019 IEEE International Geoscience and Remote Sensing Symposium*, pages 1454–1457. IEEE, 2019. 2, 3, 6, 7, 8, 15
- [73] Satoshi Suzuki et al. Topological structural analysis of digitized binary images by border following. *Computer vision, graphics, and image processing*, 30(1):32–46, 1985. 5
- [74] Luming Tang, Menglin Jia, Qianqian Wang, Cheng Perng Phoo, and Bharath Hariharan. Emergent correspondence from image diffusion. *Advances in Neural Information Processing Systems*, 36:1363–1389, 2023. 2
- [75] Juan Terven, Diana-Margarita Córdova-Esparza, and Julio-Alejandro Romero-González. A comprehensive review of yolo architectures in computer vision: From yolov1 to yolov8 and yolo-nas. *Machine Learning and Knowledge Extraction*, 5(4):1680–1716, 2023. 2
- [76] Zhuotao Tian, Hengshuang Zhao, Michelle Shu, Zhicheng Yang, Ruiyu Li, and Jiaya Jia. Prior guided feature enrichment network for few-shot segmentation. *IEEE transactions on pattern analysis and machine intelligence*, 44(2):1050–1065, 2020. 14
- [77] Kaixin Wang, Jun Hao Liew, Yingtian Zou, Daquan Zhou, and Jiashi Feng. Panet: Few-shot image semantic segmentation with prototype alignment. In *proceedings of the IEEE/CVF international conference on computer vision*, pages 9197–9206, 2019. 7, 14
- [78] Xinlong Wang, Wen Wang, Yue Cao, Chunhua Shen, and Tiejun Huang. Images speak in images: A generalist painter for in-context visual learning. In *Proceedings of the IEEE/CVF Conference on Computer Vision and Pattern Recognition*, pages 6830–6839, 2023. 2, 3, 7, 8
- [79] Xinlong Wang, Xiaosong Zhang, Yue Cao, Wen Wang, Chunhua Shen, and Tiejun Huang. Seggpt: Towards segmenting everything in context. In *Proceedings of the IEEE/CVF International Conference on Computer Vision*, pages 1130–1140, 2023. 2, 3, 7, 8
- [80] Sanghyun Woo, Shoubhik Debnath, Ronghang Hu, Xinlei Chen, Zhuang Liu, In So Kweon, and Saining Xie. Convnext v2: Co-designing and scaling convnets with masked autoencoders. In *Proceedings of the IEEE/CVF Conference on Computer Vision and Pattern Recognition*, pages 16133–16142, 2023. 2
- [81] Yuxin Wu and Kaiming He. Group normalization. In *Proceedings of the European conference on computer vision (ECCV)*, pages 3–19, 2018. 5
- [82] Jiahui Yu, Zirui Wang, Vijay Vasudevan, Legg Yeung, Mojtaba Seyedhosseini, and Yonghui Wu. Coca: Contrastive captioners are image-text foundation models. *arXiv preprint arXiv:2205.01917*, 2022. 3
- [83] Chi Zhang, Guosheng Lin, Fayao Liu, Jiushuang Guo, Qingyao Wu, and Rui Yao. Pyramid graph networks with connection attentions for region-based one-shot semantic segmentation. In *Proceedings of the IEEE/CVF International Conference on Computer Vision*, pages 9587–9595, 2019. 14
- [84] Haojie Zhang, Yongyi Su, Xun Xu, and Kui Jia. Improving the generalization of segmentation foundation model under distribution shift via weakly supervised adaptation. In *Proceedings of the IEEE/CVF Conference on Computer Vision and Pattern Recognition*, pages 23385–23395, 2024. 7
- [85] Jian-Wei Zhang, Yifan Sun, Yi Yang, and Wei Chen. Feature-proxy transformer for few-shot segmentation. *Advances in neural information processing systems*, 35:6575–6588, 2022. 1, 3, 8
- [86] Renrui Zhang, Zhengkai Jiang, Ziyu Guo, Shilin Yan, Junting Pan, Xianzheng Ma, Hao Dong, Peng Gao, and Hongsheng Li. Personalize segment anything model with one shot. *arXiv preprint arXiv:2305.03048*, 2023. 2, 3, 6, 7, 13, 15
- [87] Hengshuang Zhao, Jianping Shi, Xiaojuan Qi, Xiaogang Wang, and Jiaya Jia. Pyramid scene parsing network. In *Proceedings of the IEEE conference on computer vision and pattern recognition*, pages 2881–2890, 2017. 7
- [88] L Zhu, P Tilke, S Nagendra, M Etchebes, and M LeFranc. A rapid and realistic 3d stratigraphic model generator conditioned on reference well log data. In *Second EAGE Digitalization Conference and Exhibition*, pages 1–5. European Association of Geoscientists & Engineers, 2022. 3
- [89] Xizhou Zhu, Weijie Su, Lewei Lu, Bin Li, Xiaogang Wang, and Jifeng Dai. Deformable detr: Deformable transformers for end-to-end object detection. *arXiv preprint arXiv:2010.04159*, 2020. 2

Appendix

A. Additional qualitative analysis of embedding similarity approaches

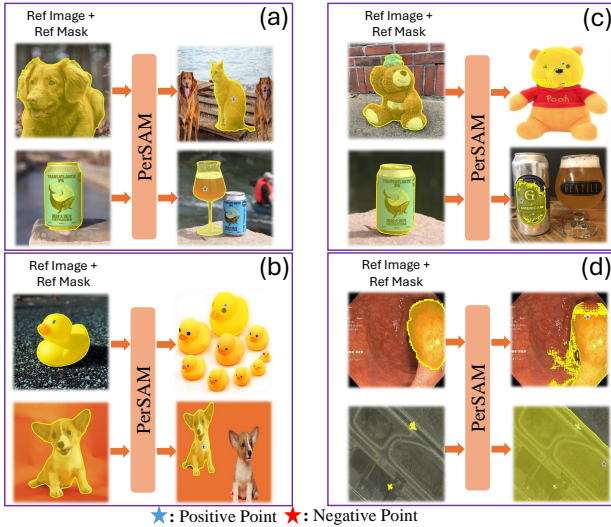


Figure 8. Illustration of key limitations of training-free, embedding similarity-based spatial prompt engineering methods.

To further examine the limitations of similarity-based methods, we conduct extensive empirical experiments using PerSAM [86] as the test bed, as shown in Figure 8. PerSAM generates positive (★) and negative (★) point prompts based on an in-context sample consisting of an image and its mask. Our experiments reveal the following key issues: (i) *Susceptibility to visual distractions*—demonstrated in Figure 8(a), where correspondence maps may highlight unrelated objects sharing similar features, and positive prompts are often biased toward the image center. (ii) *Poor generalization*—as shown in Figure 8(b), where objects with different visual features fail to be detected despite belonging to the same category. (iii) *Inability to handle multiple instances*—highlighted in Figure 8(c), where only one instance is typically identified when multiple are present. (iv) *Suboptimal performance on domain-specific tasks*—such as medical or remote sensing segmentation (Figure 8(d)). This occurs because (1) generic pre-trained VFMs lack training on domain-specific data, leading to inadequate embeddings, and (2) a single pair of positive-negative prompts results in ambiguous segmentation, as noted in the SAM paper [35].

These findings suggest that relying solely on generic pre-trained VFMs for embedding extraction and using similarity between in-context samples and target images leads to sub-optimal prompt generation. Such methods fail to produce task-specific spatial prompts needed for accurately defin-

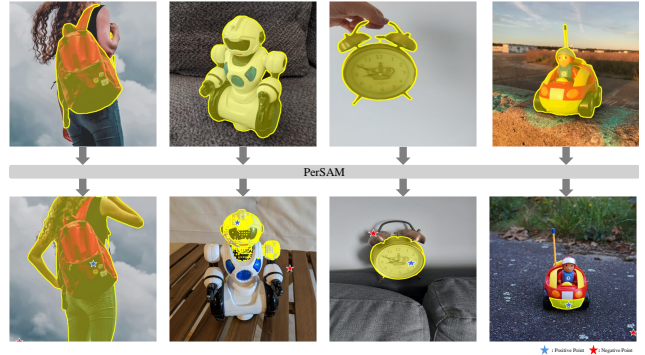


Figure 9. Illustration of poor segmentation from insufficient or unclear point prompts. Results from PerSAM [86] show that a single point prompt is insufficient for robust segmentation.

ing object boundaries, differentiating instances, and grouping semantic regions. They also struggle with complex scenes containing multiple objects, varying scales, and occlusions, where generic embeddings lack precision for fine-grained details. Moreover, these approaches often overlook context-specific variations, such as domain-specific textures or unique object features, and cannot adapt effectively to dynamic scenes or novel objects not seen during training. SAMIC addresses these limitations by learning dense visual correspondences between in-context samples and target images, enabling the generation of more effective, task-specific spatial point prompts tailored to each downstream segmentation task.

B. Design of SAMBOX

SAM’s ambiguity problem arises when provided prompts are unclear or insufficient, leading to misinterpretation, especially in scenarios with multiple objects, unclear boundaries, or occlusions. As illustrated in Figure 8(c) and Figure 9, segmentation masks predicted by PerSAM [35] show that inadequate prompts often cause SAM to segment only parts of objects or include multiple objects.

To ensure robust data collection, understanding SAM’s internal mechanisms, particularly how it processes spatial prompts to generate segmentation masks, is crucial. SAM [35] features an architecture with an image encoder that generates embeddings, a prompt encoder that processes user inputs, and a lightweight mask decoder that integrates both to predict segmentation masks. SAM is designed to generate a valid mask for any prompt, even ambiguous ones. For instance, a point on a shirt might correspond to either the shirt or the person wearing it. In such cases, SAM produces three masks, ranks them based on predicted confidence scores, and selects the mask with the highest score.

As noted by the authors of the SAM paper [35], SAM’s

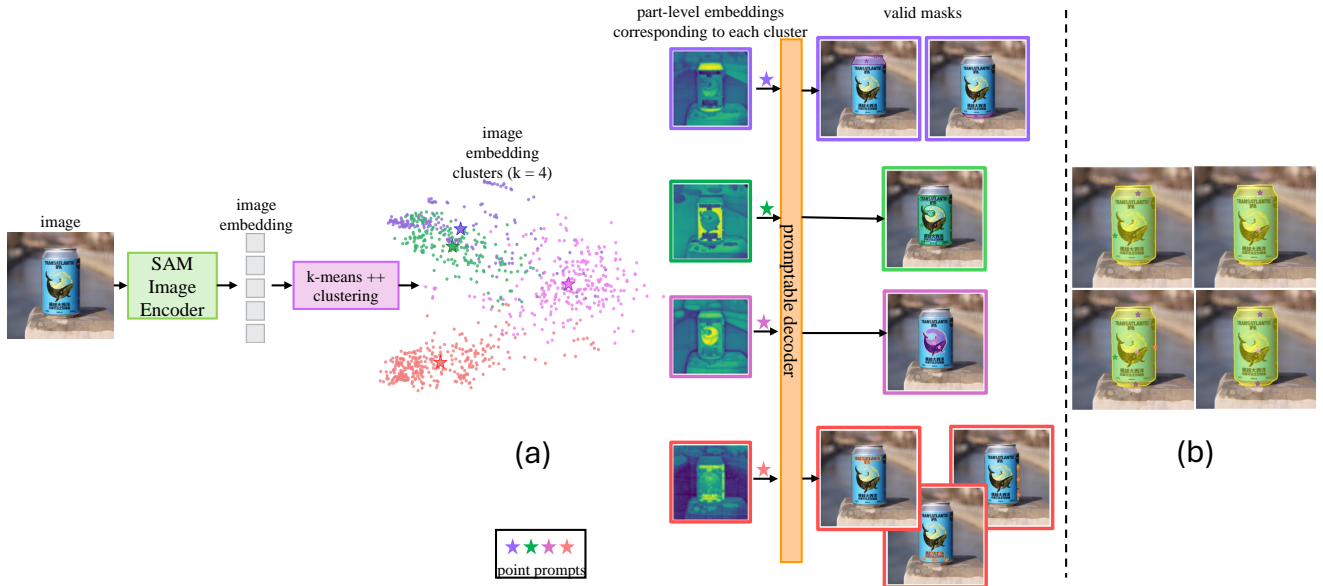


Figure 10. (a) Illustration of SAM’s ambiguity-aware design. When the image embedding from SAM is clustered, we get part-level embeddings which represents different textures, colors and text features. A point prompt sampled from one of the clusters would segment only part of the object, leading to ambiguity. This is a byproduct of SAM’s design. **(b) Combination of spatial prompt points corresponding to two or more part-level embeddings.** This figure demonstrates why multiple point prompts are necessary for robust segmentation of objects of interest.

ambiguity decreases with multiple prompts. We illustrate how multiple spatial point prompts help resolve SAM’s ambiguity problem in Figure 10. To begin, we pass an image through SAM’s image encoder to extract its embedding. We then apply the k-means++ algorithm [3] to cluster the image embedding into n parts. These clusters, representing part-level embeddings, are color-coded, with their corresponding centroids marked by colored stars overlaid on each identified group. When we align each cluster in the feature space with pixels in the RGB space, the bright yellow regions in each cluster become prominent. We observe that SAM’s encoder tends to group features based on color and texture, (e.g., the text characters or images on a drink can as shown). Sampling a spatial point prompt from any of the highlighted yellow regions (or from its corresponding cluster in the feature space) results in SAM generating a valid mask, typically segmenting some part of the can, as shown in Figure 10(a). However, when we combine multiple spatial point prompts from two or more clusters, SAM successfully segments the entire can, as shown in Figure 10(b).

We embed this part-aware information into SAMBOX to generate robust point prompts as ground truth. SAM assigns lower confidence scores to segmentation maps created with a single point prompt, while the confidence score increases with the addition of multiple prompts, until it eventually saturates. When users manually annotate images, they place spatial point prompts one at a time. The tool

displays the current confidence score, which updates with each new prompt. Users can stop when the score saturates, indicating that points covering multiple part-level features have been sampled. This process enables SAMIC to learn task-specific, ambiguity-aware spatial point prompts.

C. Additional Ablation Study

Methods	pascal-5 ^t										# learnable parameters
	1-shot					5-shot					
	5 ⁰	5 ¹	5 ²	5 ³	mean	5 ⁰	5 ¹	5 ²	5 ³	mean	
PANet [77]	44.0	57.5	50.8	33.5	40.8	55.3	67.2	61.3	53.2	59.3	23.5M
PGNet [83]	56.0	66.9	50.6	32.4	41.1	57.7	68.7	52.9	54.6	58.5	17.2M
PPNet [42]	48.6	60.6	55.7	34.7	43.4	58.9	68.3	66.8	58.0	63.0	31.5M
PFENet [76]	61.7	69.5	55.4	41.2	48.1	63.1	70.7	55.8	57.9	61.9	10.8M
RePRI [7]	59.8	68.3	62.1	52.4	58.0	64.6	71.4	71.1	59.3	66.6	-
HSNet [47]	64.3	70.7	60.3	54.0	59.1	70.3	73.2	67.4	67.1	69.5	2.6M

Table 7. Choosing the few-shot learner for SAMIC.

Choosing Few-shot learner. The design of SAMIC requires it to interpret diverse visual cues and establish precise correspondences between a limited set of in-context samples and target images. Furthermore, we prioritize computational efficiency and fast convergence for SAMIC, making a few-shot learning approach essential. To meet these needs, we chose convolutional architectures, which offer greater efficiency compared to larger transformer-based models. As shown in Tab. 7, we experimented with multiple convolutional few-shot learners and HSNet [47] performed the best among them.

D. Additional Qualitative Results

We demonstrate SAMIC’s effectiveness on diverse downstream tasks through additional qualitative results as shown in Figure 11, Figure 12 and Figure 13. It can be observed that SAMIC outperforms contemporary spatial prompt engineering methods PerSAM [86] and Matcher [44] on PerSeg [68] and NWPU VHR-10 [72] datasets.

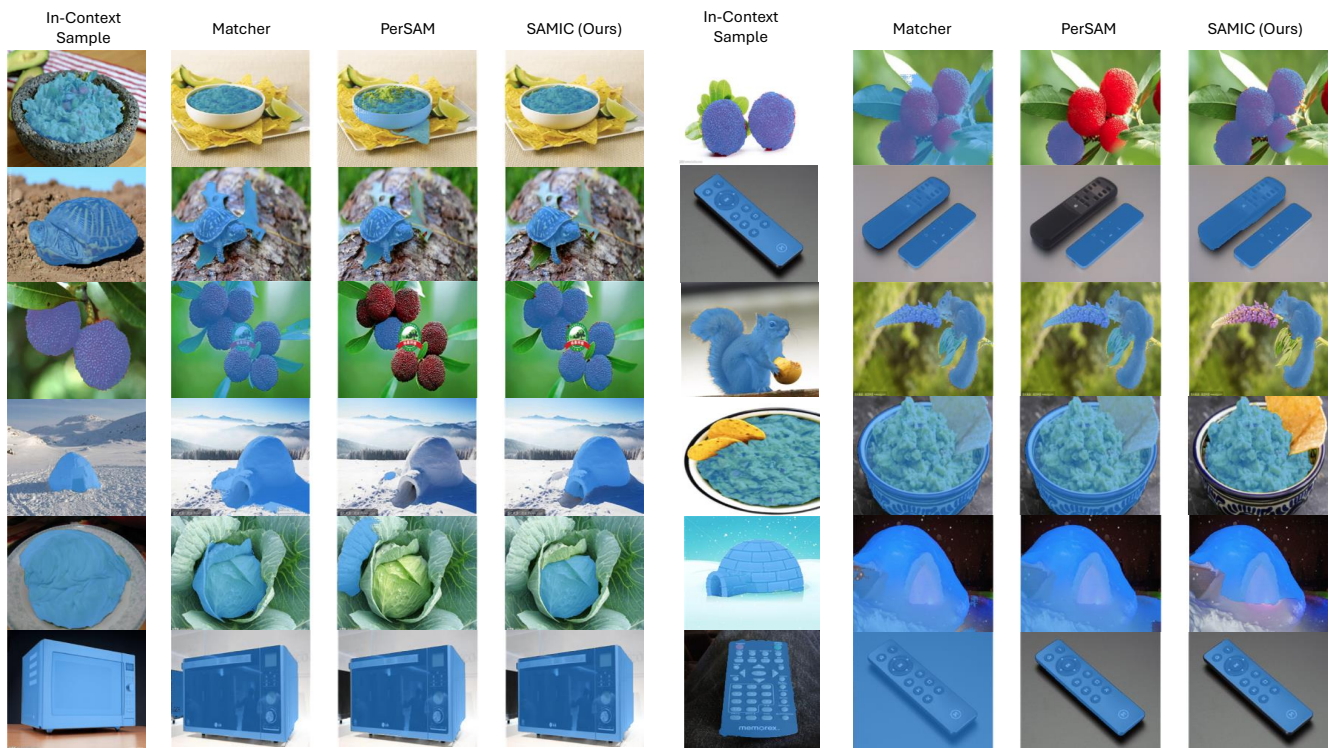


Figure 11. Qualitative results of SAMIC compared with Matcher and PerSAM on PerSeg dataset.

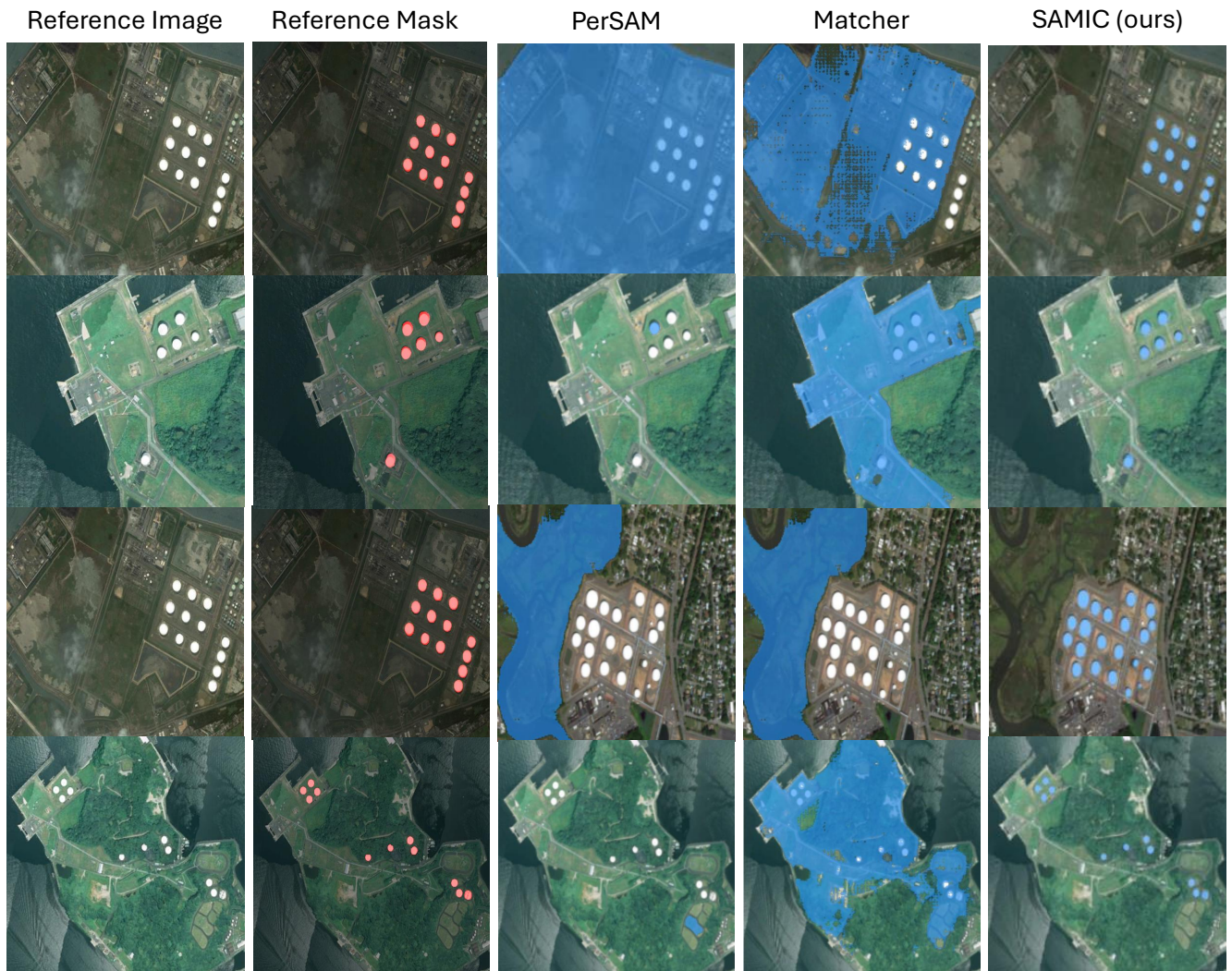


Figure 12. Qualitative results of SAMIC compared with Matcher and PerSAM on the tanks class from NWPU VHR-10 dataset.

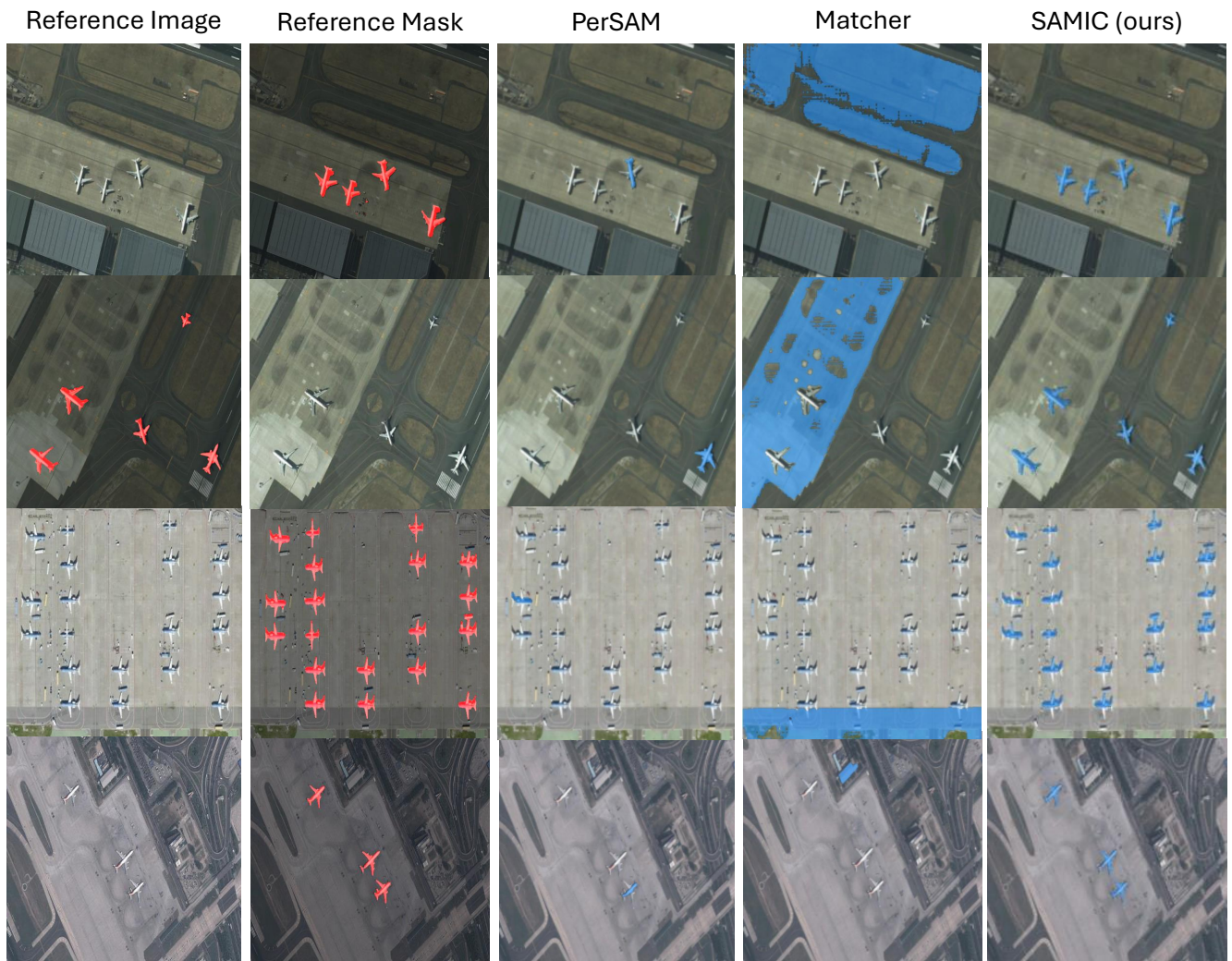


Figure 13. Qualitative results of SAMIC compared with Matcher and PerSAM on the airplane class from NWPU VHR-10 dataset.